hInt. J. Electrochem. Sci., 13 **(2018)** 631 – 641, doi: 10.20964/2018.01.64

International Journal of
ELECTROCHEMICAL
SCIENCE
www.electrochemsci.org

Corrosion behavior of AISI 316L stainless steel in a NaOH-H_2O mixture.

Y.R Galindo-Luna[1], *A. Torres-Islas*[2,*], *R.J. Romero*[3], *M. Montiel-González*[2] *and S. Serna*[3]

[1] Posgrado en Investigación en Ingeniería y Ciencias Aplicadas, Universidad Autónoma del Estado de Morelos, Av. Universidad 1001, Col. Chamilpa, C.P. 62209, Cuernavaca, Morelos, México.
[2] Facultad de Ciencias Químicas e Ingeniería P.A. Ing. Mecánica, Universidad Autónoma del Estado de Morelos, Av. Universidad 1001, Col. Chamilpa, C.P. 62209, Cuernavaca, Morelos, México.
[3] Centro de Investigación en Ingeniería y Ciencias Aplicadas, Universidad Autónoma del Estado de Morelos, Av. Universidad 1001, Col. Chamilpa, C.P. 62209, Cuernavaca, Morelos, México.
[*]E-mail: alvaro.torres@uaem.mx

Received: 5 September 2017 / *Accepted:* 15 November 2017 / *Published:* 16 December 2017

Potentiodynamic polarization analysis and electrochemical impedance spectroscopy, were used to determine the corrosion rate AISI 316L stainless steel (316L) in a NaOH-H_2O working air-conditioning mixture. The aqueous concentrations were 40% and 50% (w/w), temperature was set at 35°C and 90°C (similar to the conditions of the absorber and generator in an absorption air-conditioning system). The results showed that the material exhibited a passivation region in all cases, and the corrosion mechanism was dominated by charge transfer. Additionally, at 35°C and 90°C the corrosion process was mainly influenced by the concentration and temperature of the solution. The results were attributed to the steel chemical composition, the chemical stability of the corrosion products, the structural state of the passive film, and the ability to prevent the diffusion of metal ions. According to the results, the NaOH-H_2O mixture possesses electrochemical characteristics that permit its application as a working fluid for air-conditioning absorption processes.

Keywords: Absorption systems, NaOH-H_2O solutions, Stainless steel AISI 316L, Corrosion resistance.

1. INTRODUCTION

The main goal of absorption heat pump devices is to mitigate the negative environmental impacts of burning of fossil fuels. The air-conditioning absorption system (ACAS) represents an important energy saving method, because it is driven by industrial waste heat or renewable energy [1, 2]. The absorption air-conditioning technology consists of an evaporator, a condenser, a generator and an absorber. The absorber is the primary-component in an absorption system because it is the main

limiting factor for increasing the performance, and determines the size and cost of the system [3]. The performance of an absorption cycle is dependent on the chemical and thermodynamic properties of the working mixture [4]. The working mixture is composed of a refrigerant and an absorbent. The refrigerant flows into the condenser and the evaporator, where it undergoes a phase change (from gas to liquid); the absorbent solution undergoes concentration changes in the generator and absorber. In the absorber, the concentrated working mixture (pumped from the generator) absorbs the working fluid vapor (coming from the evaporator); this absorption process delivers a heat load at low temperatures (close to the ambient temperature) and produces a diluted solution stream (in the absorbent) [5]. Conventional working mixtures are mainly ammonia-water and lithium bromide-water; however, they have great disadvantages, such as high toxicity, easy crystallization and extensive corrosion [6]. Therefore, the use of $NaOH_2$-H_2O as a working fluid in the absorption process is proposed as an alternative. According to the theoretical analysis, this mixture shows a coefficient of performance (COP) on the same order as those of conventional mixtures for the absorption cycle [7-10]. Several authors have reported on the chemical and thermochemical behavior of this mixture, including its absorption-desorption properties, sorption capability and dynamic compression [11-14]. However, the corrosion behavior as a function of temperature and concentration of the $NaOH_2$-H_2O mixture (operating conditions) has not been reported. This aspect is important because the piping and devices used in the absorption process are made of AISI 316L stainless steel.

In this work, the corrosion behavior of AISI 316L stainless steel (316L SS) in $NaOH_2$-H_2O solutions under the operating conditions of certain components such as the absorber and generator, were analyzed. The analysis was supported by potentiodynamic polarization (PP) and electrochemical impedance spectroscopy (EIS) measurements. In addition, scanning electron microscopy (SEM) characterization was performed.

2. EXPERIMENTAL PROCEDURES

The chemical composition of the 316L SS in wt% was 0.030-C, 2.0-Mn, 0.045-P, 0.030-S, 0.75-Si, 16.0-Cr, 10.2-Ni, 2.3-Mo, 0.08-N, and Fe balance. The test specimens were cut to a 1 cm^2 exposed area and encapsulated in epoxy resin. Before testing, the specimens were abraded longitudinally with 600-grade emery paper, degreased with methyl alcohol and dried under air. The electrochemical cell test consisted of a three-electrode arrangement; silver/silver chloride (Ag/AgCl) as the reference, a graphite bar as the counter electrode and the 316L SS sample as the working electrode, using a fully automated potentiostat controlled by a desk top computer. The NaOH-H_2O test solutions were prepared from analytical grade reagents at 40% and 50% concentrations. The electrochemical techniques employed for the corrosion tests were potentiodynamic polarization analysis and electrochemical impedance spectroscopy (EIS). The potentiodynamic polarization curves were collected in a potential window from -1000 to 1000 mV at a sweep rate of 1.0 mV/s. The values of the corrosion current density were calculated using the Tafel extrapolation method by;, considering an extrapolation zone of 150 mV. The EIS test was performed by applying an excitation signal of ±15 mV vs. The open circuit potential, in the frequency range of 20,000 Hz to 0.1 Hz. Zview software was

used to simulate and develop the electrical circuits. The tests were performed according to the ASTM G5-94 and G59-91 standards, at 35 C° for 72-h and 90 C°, for direct elapsed time, respectively. The corrosion rate (V_{corr}) was calculated from Faraday's equation according to the ASTM G-102-89 standard.

3. RESULTS AND DISCUSSION

Figure 1 shows the 316L SS polarization curves in contact with the NaOH solutions with concentrations of 40% and 50% at 35°C and 90°C respectively. It is observed that at 35°C there is a great difference in the corrosion potential (E_{corr}) as it is more anodic in the conditions of 50% concentration (50%) than 40% concentration (40%), with values of -1124 mV and -788 mV respectively, as shown in the corrosion parameters listed in Table 1.

On the other hand, at 90°C, the variation in the E_{corr} as a function of the concentration is practically null with a -631 mV value for both concentrations, which is more cathodic than that at 35°C. The corrosion current density (I_{corr}) for 35°C and 90°C increases when the concentration of the aqueous solution also increases. For 40% and 35°C conditions, the corrosion rate was 0.0045 mA/cm^2 and for the 50% and 90°C conditions, it was 0.0206 mA/cm^2 (Table 1).

Table 1. Potentiodynamic polarization curve parameters.

Concentration-temperature NaOH	E_{corr} (mV)	I_{corr} (mA/cm^2)	E_{pass} (mV)	E_{pitt} (mV)	V_{corr} (mm/year)
40% -35°C	-788	0.0045	-710	-376	0.05
50% -35°C	-1124	0.0164	-853	-264	0.17
40% -90°C	-631	0.0156	-248	135	0.16
50% -90°C	-631	0.0206	-263	77	0.21

In the polarization curves, it is also observed that for all conditions (except for 50% at 35°C) there is a passivity zone preceded by a zone of transpassivity, which is relatively short. In general, considering the differences in the E_{corr} values for all conditions, it is observed that the passive zone exhibits approximately the same permanence range before the pitting potential (E_{pitt}). However, at 90°C before reaching the condition of transpassivity-passivity, the anodic branch in both concentrations exhibit higher values of E_{pitt} and corrosion rate than at 35°C, as seen in the data provided in Table 1.

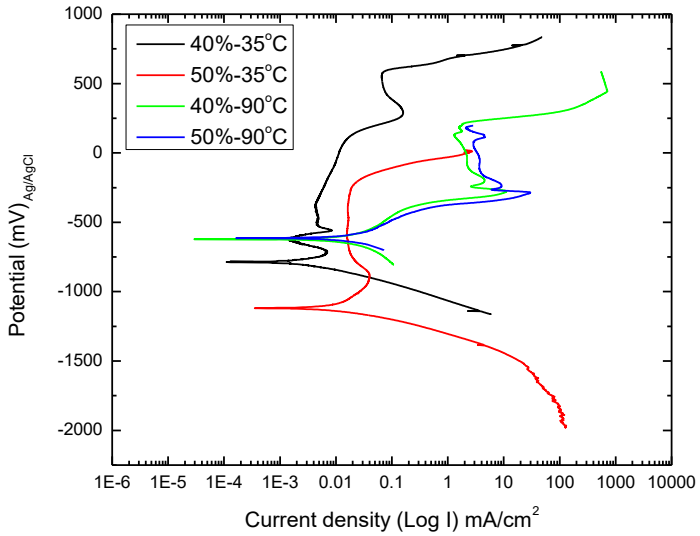

Figure 1. Potentiodynamic polarization curves of 316L SS in aqueous solutions, with 40% and 50% NaOH concentrations, at 35°C and 90°C.

The E_{corr} difference between the 40% - 35°C and 50% - 35°C conditions, indicates that the NaOH concentration plays a fundamental role in the rate of the cathodic and anodic reactions before reaching the thermodynamic equilibrium; therefore when the passive chromium oxide film breaks down, it allows the steel to oxidize [15]. Then, the reaction $Fe^{2\pm} + 2NaOH \rightarrow Fe(OH)_2 + 2Na^+$ represents the mass balance and even the energy balance of the system under study, Stoichiometric relations usually provide to a general description of the process, since in reality elemental reactions from intermediate compounds that govern the reaction velocity even though they do not influence the final chemical equilibrium. Therefore, when the NaOH concentration increases, the reduction reactions (cathodic), together with the elemental reactions, enhance the hydrogen evolution reaction in accordance with $O_2 + 2H_2O + 4e^- \rightarrow 4OH^-$ in alkaline solutions, reaching the E_{corr} at cathodic values. This mechanism was discusse by Betova et al. [16]. Moreover, according to Cuevas et al., [17] at low temperatures, the E_{corr} for 316L SS shows low activity, due to the presence of elements such as: Cr, Ni and Mo.

For the conditions 40% - 90°C and 50% - 90°C, the E_{corr} is anodic, because that elemental reactions increase the formation kinetic energy when the temperature increases [18]. The above is a result of the reactions and less stable compounds that delay the equilibrium in the red-ox reactions and the transpassivation-passivation zone formation, as suggested by Zhang et al.[19].

Figure 2 shows the Nyquist plots corresponding to the 40% - 35°C and 50% - 35°C EIS tests.

Figure 2a shows that at 40% NaOH, the Nyquist graphs present a nearly straight line (a 'constant phase' impedance) with a barely perceptible tendency to form a semicircle. This behavior is related to a charge transfer process that is highly capacitive [20, 21] as seen in the values on the order of 10000 $\Omega.cm^2$ for the impedance module |Z| in the bode plot (Figure 3a)

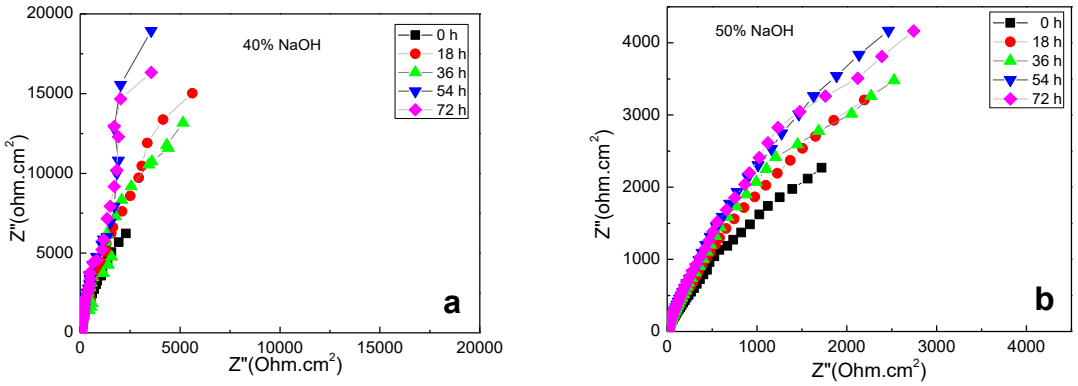

Figure 2. Nyquist plots for 316L SS, after exposure for 72 hours to (a) 50% and (b) 40% NaOH at 35°C.

In Figure 2b, the Nyquist plots for 50% NaOH have a well-defined tendency to form a semicircle, which indicates that there is also a charge transfer process, with |Z| values on the order of 1000 Ω.cm^2. (Figure 3b).

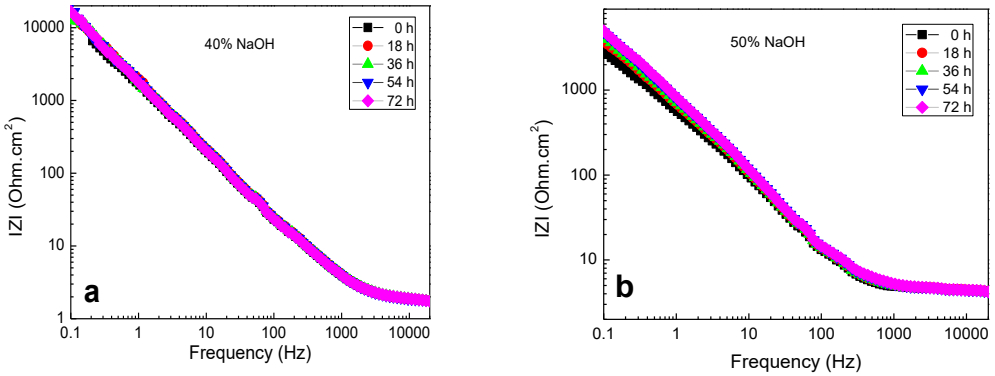

Figure 3. Bode plots for 316L SS, after to exposure for 72 hours to (a) 50% and (b) 40% NaOH at 35°C.

Figure 3 show that |Z| in both concentrations is not greatly affected by the exposure time. However, the concentration and temperature play an important role in the individual corrosion mechanism, as described below.

The parameters of the EIS tests simulated in the Zview software for the conditions at 35°C are shown in Tables 2 and 3, respectively. The parameter results, show that the charge transfer resistance (R_{ct}) is lower in the 40% solution than in the 50% solution, this means that the capacitance of the double layer should have lower values of |Z| in the 40% solution than in the 50% solution. However, as mentioned above, the opposite behavior is observed, which indicates that the charge transfer gradient in the double layer in the 40% condition is greater than in the 50% condition. Therefore, the data presented here provide strong evidence for the presence of passive layer in the 40% condition that is less protective and relatively permeable.

Table 2. Simulation parameters for 316L SS, after exposure for 72 h to 40% NaOH at 35°C.

Exposure time	R_s ($\Omega.cm^2$)	CPEcdl ($\Omega^{-1}Xs^{-n}Xcm^{-2}$)	R_{ct} ($\Omega.cm^2$)	n -----
0 h	1.816	$1.14E^{-4}$	21.4	0.9
18 h	1.816	$1.14E^{-4}$	230.9	0.9
36 h	1.796	$9.10E^{-5}$	99.68	0.9
54 h	1.841	$7.29E^{-5}$	48.45	0.9
72 h	1.829	$8.00E^{-5}$	47.38	0.9

Table 3. Simulation parameters for AISI 316 SS, after to exposure for 72 h to 50% NaOH at 35°C.

Exposure time	R_s ($\Omega.cm^2$)	CPEcdl ($\Omega^{-1}Xs^{-n}Xcm^{-2}$)	R_{ct} ($\Omega.cm^2$)	n -----
0 h	4.548	$1.92E^{-4}$	436.7	0.9
18 h	4.675	$1.81E^{-4}$	838.6	0.9
36 h	4.542	$1.82E^{-4}$	1,207	0.9
54 h	4.719	$1.83E^{-4}$	1,720	0.9
72 h	4.705	$1.88E^{-4}$	2,408	0.9

The previous statement is supported by the polarization curve at 40% shown in Figure 1. In this figure, after the transpassivation zone, a short passivation zone exists, and then the behavior of continued dissolution is recorded, finally reaching another transpassivation zone. This phenomenon is due to the presence of a permeable layer on the surface of the material that does not generate passivation, therefore the flow of ions towards the solution due to the continuous decreases its solution resistance (R_s), relative to that of the 50% condition, as shown in the R_s data provided in Tables 2 and 3 respectively.

In the 50% condition, the difference in the |Z| values indicates that R_{ct} should be lower than that in the 40% condition. However, the simulated values of 50% R_{ct} given in Table 3 show a one order of magnitude increase. This means that a layer that prevents ion transfer to the solution is formed on the steel surface. This aspect agrees well with the 50% polarization curve passivation (Figure 1), and the increase in R_s (Table 3).

As reported in the review article by Allen et al. [22] the structure of the passive layer on austenitic stainless steels consist of an inner layer, and an outer layer. Which layer has an affinity for Fe, Cr or Ni depends on the pH of the solution and the content of ions, so the difference in the corrosion rates of the 40% and 50% condition indicate the amount of metal lost from the steel. This material can remain on the surface a metal oxide layer, or dissolve into the solution. When dissolved, the metal ions released into the solution, change the solution pH. Thus, it can be assumed that an oxide layer formed and variation of the solution pH could affect the chemical structures of the inner and, outer layers and consequently, the charger transfer characteristics of the 50% and 40% conditions. These results are in agreement with those obtained by Svishchev et al.[23].

In Figure 4, the Bode plots show characteristics of each behavior previously described. Figure 4a shows that in the frequency range from 10000 Hz to 5000 Hz for the 40% concentration, the phase

angle decreases, approaching zero approximately 5000 Hz. The angle increases to 80 degrees at 25 Hz and finally, from 80 degrees, it diminishes with decreasing frequency to 60 degrees at 0.1 Hz. This behavior of the phase angle at high frequencies is related to the instability of the passive layer. These results were compared with those from other literatures reports [16] in which the passive film exhibits transpassivated events at the beginning of the anodic branch such in the polarization curves similar to those observed in the 40% polarization curve (Figure 1).

On the other hand, the Bode plot of the 50% concentration displayed in Figure 4b, shows a phase angle value of 15 degrees at 1000 Hz, which gradually increases to reach the maximum gap at 100 Hz with an 85 degree value. The angle remains stable in this range, until the frequency reaches 3 Hz; after this frequency and up to 0.1 Hz, a random variation in the phase angle is observed. This behavior is in accordance with the progress in the anodic branch of the polarization curve for the 50% concentration. In the beginning this curve is passive and remains passive until its breakdown.

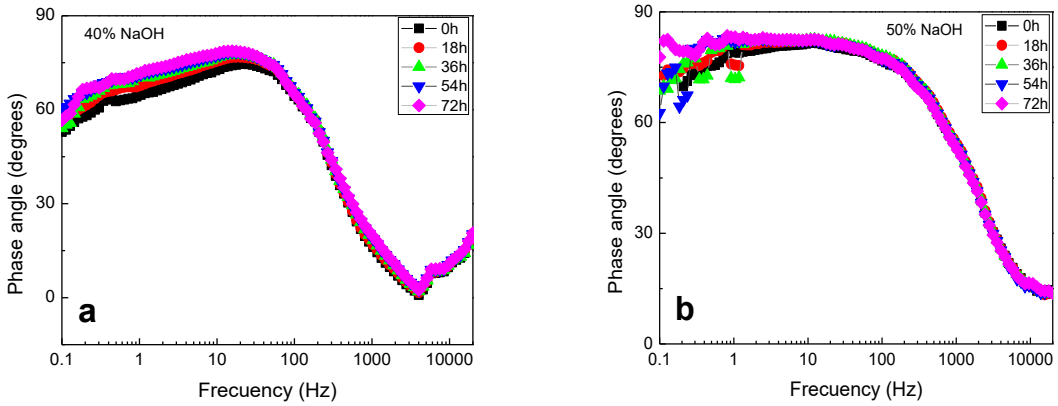

Figure 4. Bode plot phase angle for 316L SS, after exposure for 72 h in (a) 40% and (b) 50% NaOH at 35°C.

Moreover, at 90°C, independently of the concentration, the results indicate that the temperature plays an important role in the behavior of the stainless-steel corrosion rate. Figure 5 shows the Nyquist plot for the 40% and 50% concentrations. In this figure, the formation of 2 semicircles, with significantly different |Z| values can be seen. Figure 6a shows that the difference is of one order of magnitude, for the 40% and 50% concentrations, the values are 1700 $\Omega.cm^2$ and 250 $\Omega.cm^2$, respectively as shown in Figure 6b. However, in the polarization curves, the anodic branches of both concentrations exhibit similar behaviors in the passivity zone, which means that the composition of the corrosion products present in the protective film are different and therefore interact differently during the charge transfer process, according to Behnamian [20]. Nevertheless, in both concentrations the passive film protects the steel in this zone.

It is known that alloying elements and impurities can change the oxidation and corrosion susceptibility of the base metal at high temperatures. In Fe–Ni–Cr alloys, the outward diffusion of iron and nickel and their reaction with oxygen leads to the formation of oxides, such as Fe_3O_4, Fe_2O_3, FeO, and NiO, depending on the oxygen content, temperature and exposure time [21]. Furthermore, in the pH-potential diagram for iron (Pourbaix) [24], the two concentrations coincide in the region that is the

limit between the continuous dissolution of Fe^{2+} and the $Fe(OH)_2$ passive area, which is also a determining factor in the formation and composition of the passive layer [25]. Moreover, the diffusion rate differences correspond to the Bode graph behavior (Figure 6), where at intermediate frequencies (Figure 6a), the phase angle is greater in the 40% concentration than the 50% concentration, (Figure 6b) and remains higher in the higher frequency range.

In Figure 7, the SEM micrographs show the differences in the morphologies of the corrosion products on the steel surface, after the test at 90°C. In this figure, for the concentration at 40%, the corrosion products are more homogeneous and compact than those for the concentration at 50%, which exhibit detached flakes.

The main objective of this study was to evaluate the corrosion behavior of SS316L in test NaOH–H_2O solutions. However, the results of previous studies [20, 25] and our study indicated that the composition of the passive layer generated at 35°C and 90°C contained $FeCr_2O_4$ and/ or Fe_3O_4 oxides.

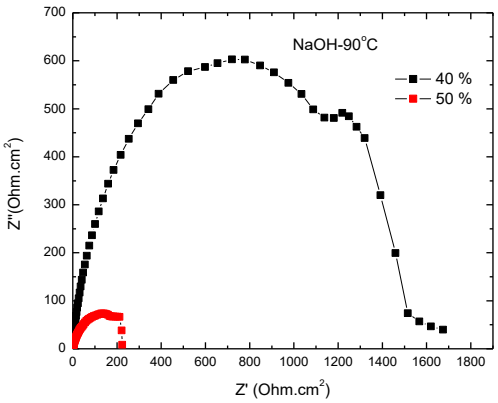

Figure 5. Nyquist plots for 316L SS, after exposure to NaOH concentrations of 50% and 40% at 90°C.

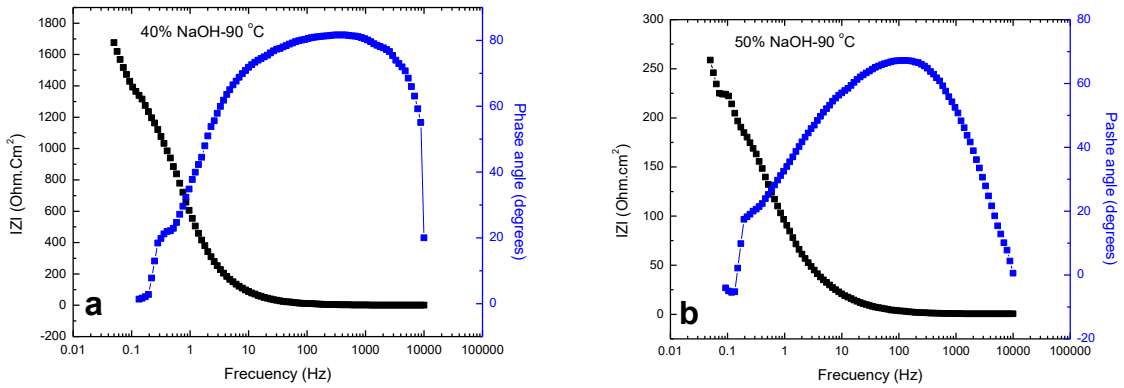

Figure 6. |Z| and phase angle Bode plots for 316L SS, after exposure to (a) 40% and (b) 50% NaOH at 90°C.

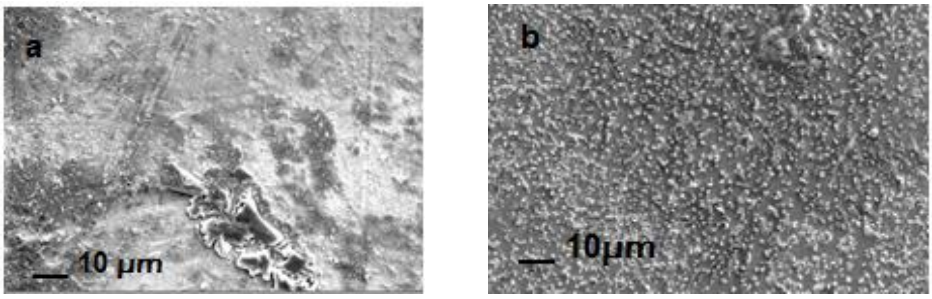

Figure 7. Surface corrosion product morphology for (a) 40% and (b) 50% NaOH at 90°C.

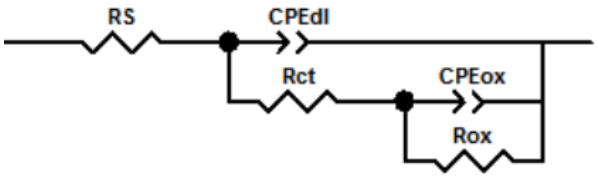

Figure 8. Equivalent circuit representing the impedance spectra for the corrosion data of 316L SS in NaOH with concentrations of 40 and 50%.

On the other hand, in the analysis of the EIS data parameters simulated, in Zview software (Table 3), the phase element (CPE) is observed. In experimental conditions there are no ideal capacitors; therefore, this element is defined by the expression:

$$Z_{CPE}= \frac{1}{Q(j\omega)^{\alpha}} \quad (1)$$

where: Q is a constant (Fs^{n-1}), ω is the angular frequency, j is an imaginary number, and α is an exponent with a value less than one for an element of constant phase. This constant phase element (CPE) is often related to the surface roughness of the working electrode (WE). The double layer capacitance and the capacitive loop corrosion products are represented by the equivalent circuit displayed in Figure 8, which represents the charge transfer mechanism proposed according to the obtained results.

Table 4. Comparison of the corrosion parameters for SS316L and SS316 in NaOH solutions reported by various authors those from our results.

Reference	Material	Temp °C	I_{corr} (mA/cm^2)
Our results	SS316L	40%-35°C	0.0045
	SS316L	50%-35°C	0.0164
	SS316L	40%-90°C	0.0156
	SS316L	50%-90°C	0.0206
Steiu [8]	SS316	25°C	0.0015
Anaee [18]	SS316L	40°C	0.0862
	SS316L	50°C	0.0998
	SS316L	60°C	0.221
Kumar [26]	SS316L	37°C	0.0088

Finally, our results of the corrosion current density and consequent corrosion velocity under ambient working conditions (absorber and condenser conditions), have shown that in comparison with other conditions reported for the same material in contact with alkaline solutions, the corrosion rate is minor, as indicated by the corrosion parameters listed in table 4.

4. CONCLUSIONS

The results of the corrosion current density and consequent corrosion velocity under ambient working conditions,(absorber and condenser conditions) and the proposed concentrations, have shown that compared with other conditions reported for the same material in contact with alkaline solutions, the corrosion rate is minor.

The corrosion process of the 316L steel in contact with the NaOH-H_2O solution at 35°C was affected by the concentration of the solution, while that at 90 °C was affected by the temperature. The corrosion mechanism for the 40% and 50% concentrations was dominated by charge transfer, and the formation and permanence of the passive layer were attributed to the steel chemical composition, the chemical stability of the corrosion products, the structural state of the passive film, and the ability to prevent the diffusion of metal ions. The electrochemical characteristics of the solution allow it to be used as a working fluid in absorption air-conditioning systems with a coefficient of performance (COP) on the same order as that of conventional mixtures for the absorption cycle.

ACKNOWLEDGMENTS
The present study was supported by projects CB-167434 and CEMIE-SOL-09and funded by Fondo Sectorial CONACYT-SENER-Sustentabilidad Energética de México and CONACYT – Mexico.

References

1. M. Zeyghami, D. Yogi Goswami and E. Stefanakos, *Renew. Sust. Energ. Rev.*, 51 (2015) 1428.
2. J. Sun, L. Fu and S. Zhang, *Renew. Sust. Energ. Rev.*, 16 (2012) 1899.
3. J. Ibarra-Bahena, and R.J. Romero, *Energies.*, 7 (2014) 751.
4. H. Perez-Blanco, *Int. J. Refrig.*, 7 (1984) 115.
5. I. Sarbu, and C. Sebarchievici, *Energy Build.*, 67 (2013) 286.
6. X.L. Yuan, X.D. Zhang, X.L. Li , H.Q. Fan and Z.C. Zhao, *Corros. Eng. Sci. Techn.*, 48 (2013) 388.
7. P. Srikhirin , S. Aphornratana, S. Chungpaibulpatana, *Renew. Sust. Energ. Rev.*, 5 (2001) 343.
8. S. Steiu, D. Salavera, J. C. Bruno, and A. Coronas, *Int. J. Refrig*.,32 (2009) 577.
9. J. Sun, L. Fu and S. Zhang, *Renew. Sust. Energ. Rev*., 16 (2012) 1899.
10. W. Wu, W. Shi, J. Wang, B. Wang and X. Li, *Appl. Energ.*, 176 (2016) 258.
11. F. Asfand and M. Bourouis, *Int. J. Refrig*., 71 (2016) 18.
12. B. Anusha and B. Chaitanya, *International Journal of Advanced Engineering Research and Science*, 4 (2017) 149.
13. X. Daguenet-Frick, P. Gantenbein, J. Müller, B. Fumey and R. Weber, *Renew. Energ*., 110 (2017) 162.
14. K. Stephan, M. Schmitt, D. Hebecker and T. Bergmann, *lnt J. Refrig*., 20 (1997) 483.

15. C.M. Abreu, M.J. Cristóbal, M.F. Montemor, X.R. No´voa, G. Pena and M.C. Pérez, *Electrochim. Acta*, 47 (2002) 2271.
16. I. Betova , M. Bojinov , O. Hyökyvirta, T. Saario, *Corros. Sci.,* 52 (2010) 1499.
17. C. Cuevas Arteaga, J. Porcayo Calderón, C. F. Campos Sedano and J. A. Rodríguez, *Int. J. Electrochem. Sci.*, 7 (2012) 445.
18. R. A. Anaee, A. M. Al-Ghaban, *Al-Khwarizmi Eng. J.,* 11 (2015) 12.
19. B. Zhang, S. Hao, J. Wu, X. Li, C. Li, X. Di, Y. Huang, *Mater. Charact.,*131 (2017) 168.
20. C. Behnamian, A. Mostafaei, A. Kohandehghan, B. S. Amirkhiz, D. Serate, Y. Sun, S. Liu, E. Aghaie, Y. Zeng, M. Chmielus, W. Zheng, D. Guzonas, W. Chen, J. Li Luo, *Corros. Sci.,* 106 (2016) 188.
21. I Nicic, D. D. Macdonald, *J. Nucl. Mater.,* 379 (2008) 54.
22. T.R. Allen, Y. Chen, D. Guzonas, X. Ren, K. Sridharan, L. Tan, G.S. Was, E. West, *Compr. Nucl. Mater.,* 5.12 (2012) 279.
23. I.M. Svishchev, R.A.Carvajal-Ortiz, K.I.Choudhry, D.A.Guzonas, *Corros. Sci.,* 72 (2013) 20.
24. M. Pourbaix, Atlas of Electrochemical Equilibrium in Aqueous Solutions, NACE, Houston, Tex, USA, 2nd edition, 1974.
25. H.Xu, L.Wang, D.Sun, H.Yu, *Appl. Surf. Sci.,* 351 (2015) 367.
26. D.B.Kumar, R.Nagalakshmi, Dr. K.G.Muthurajan, V. Rajasekar, S. Parthasarath, International Conference on Recent Advancement In Mechanical Engineering & Technology (ICRAMET'15), *J. Chem. Pharm. Sci.,* ISSN: 0974-2115.